From stripe to slab confinement for linearization of macromolecules in nanochannels

Zuzana Benková, *Pavol Námer* and *Peter Cifra* [*]

Polymer Institute, Slovak Academy of Sciences, Dúbravská cesta 9, 845 41 Bratislava,

Slovakia

Abstract

We have investigated recently suggested advantageous analysis in the chain

linearization experiments with macromolecules confined in a stripe-like channel (Huang and

Battacharya, *Europhysics Letters* **2014**, *106*, 18004) using Monte Carlo simulations. The

enhanced chain extension in a stripe which is due to the significant excluded volume

interactions between monomers in two dimensions weakens considerably on transition to an

experimentally feasible slit-like channel. Based on the chain extension-confinement strength

dependence and the structure factor behavior for a chain in a stripe we infer the excluded

volume regime (de Gennes regime) typical for two-dimensional systems. On widening of the

stripe in direction perpendicular to the stripe plane, *i.e.* on the transition to the slab geometry,

the advantageous chain extension decreases and the Gaussian regime is observed for not very

long semiflexible chains. The evidence for pseudo-ideality in confined chains is based on four

indicators: the extension curves, variation of the extension with the persistence length *P*,

estimated limits for the regimes in investigated systems and the structure factor behavior. The

slab behavior can be observed when the two-dimensional stripe (originally of one-monomer

thickness) reaches the reduced thickness *D* larger than approximately $D/P \approx 0.2$ in the third

dimension. This maximum height of a slab at which the advantage of a stripe is retained is

very low and has implications for DNA linearization experiments.

I.   Introduction

A polymer chain confined to a sufficiently long channel with dimensions smaller than the mean span chain dimensions in the bulk is stretched along the channel axis. The linearization of biopolymers such as dsDNA molecules under biaxial confinement has found important applications in single-chain experiments.[1-8] They present an efficient, nondestructive and simple way of DNA manipulation and characterization when determining its structural details in nano- and microfluidic experiments.[9,10] In order to understand the structural and dynamic properties of a single chain confined in a channel and slit a great deal of theoretical,[11-14] experimental[1,2,8,10,15] and simulation[16-33] studies have been published. Studies have shown that the chain relaxation slows down upon increasing the confinement. Earlier studies have not covered very high confinement range and have considered rather shorter chains. However, more recent studies have turned attention to longer macromolecules in strong confinement and the focus has been shifted also to the behavior of a macromolecule in a slit[29,31-34] and understanding topological properties in confined chains.[29,30] While from the theoretical and simulation viewpoint, the behavior of a polymer confined to a three-dimensional ($3d$) channel of different geometry is well characterized, it is difficult to fabricate a nanochannel of a perfect symmetric cross-section, *i.e.* a cylinder or a square channel. The experiments are usually conducted using channels of rectangular cross-sections being of a $3d$ slab form or a slit-like channel.

In addition to the chain contour length L, effective chain width w and persistence length P, the new characteristic length D defining the size of the channel cross-section appears with D being the size length of a square channel or the diameter of a cylindrical channel. The conformation of a confined chain is then the interplay of L, w, P and D. The nano- and microfluidic devices usually operate in the moderate confinement regimes with $D \geq P$ whereas the theoretical models are well elaborated for regimes with $D \ll P$ or $D \gg P$. The

existence of the intermediate regime/regimes[20] brings about more complexity in the

experimental measurements of DNA stretching carried out in $3d$ channels. On the other hand,

it has been shown recently that these regimes are absent in a $2d$ channel, *i.e.* in a stripe[27], due

to the strong chain excluded volume interactions in a $2d$ system. At the same time the chain

extension is more significant in a stripe for the same reason, what is advantageous in

linearization experiments with DNA. Thus a channel of stripe geometry seems to simplify the

analysis of the chain extension under certain experimental conditions. However, since it is

difficult to realize the experiments on the DNA extension in a stripe it is of interest to find out

which parameters, namely the maximum height of a slab, is needed to avoid the intermediate

regimes in feasible experimental situation while retaining the higher chain extension that is

characteristic for a stripe. Thus the goal is to achieve a high extension and a more

straightforward analysis in a slab with a direct transition from the strong confinement Odijk

regime[11] to the moderate confinement de Gennes regime[35] analogous to rather theoretical case

of a stripe.

The original Odijk regime[11] derived for a cylindrical geometry of a channel manifests

itself by significantly stretched conformation of a chain in the channel of $D \ll P$. In this

regime a chain is composed of rod-like fragments deflecting from the channel walls. The

characteristic deflection length $\lambda \approx (D^2 P)^{1/3}$ is the distance between two consecutive

deflection points. The relation for the longitudinal chain extension R in a cylinder[14, 22]

$$R = L\left[1 - A_1 \left(\frac{D}{P}\right)^{2/3}\right] \tag{1}$$

is extended for the case of a rectangular channel[14] of side lengths $D_y < P$ and $D_z < P$ to

$$R = L\left[1 - A_2 \frac{D_y^{2/3} + D_z^{2/3}}{P^{2/3}}\right] \tag{2}$$

Here $A_1 = 0.1701$ and $A_2 = 0.09137$ are universal numerical constants for a cylindrical and rectangular channel,[14] respectively. Eqn (2) holds not only for a slab[14] but equally well for a stripe which has been shown by the Brownian dynamics simulations.[27]

In the moderate-confinement regime known as the de Gennes regime[35] a chain is viewed as a string of self-avoiding spherical blobs each one of size D linearly arranged along the channel axis. In a semiflexible chain, the excluded volume (EV) interactions determine the organization of g monomers of size a within a blob of the size $D \approx ag^{3/(d+2)}(P/a)^{1/(d+2)}$ where d is the spatial dimension.[36] The longitudinal chain extension is than given by a linear array of the blobs as $R \approx (N/g)D$. Together this leads to

$$R \approx L \left(\frac{a}{D}\right)^{\frac{d-1}{3}} \left(\frac{P}{a}\right)^{\frac{1}{3}}$$ (3)

One can recognize $R \sim D^{-2/3}$ dependence which is often referred scaling of the longitudinal chain extension in a channel[10, 35] for $d = 3$ as well as $R \sim D^{-1/3}$ reported in a stripe[27] for $d = 2$. As mentioned the transition between the de Gennes regime and Odijk regime is not direct but is constituted of intermediate regimes, namely the extended de Gennes and transition regimes that appear according to the system parameters.[10] While the scaling relation for the extension in eqn (3) remains the same for the extended de Gennes regime it becomes different in the transition regime. Recently, new endeavors appeared in understanding of these confinement regimes,[26] as well as in understanding of the behavior in a slit under strong confinement[34] and the behavior in channels with asymmetric cross-section.[25] Further specification of regimes of confinement is analyzed and discussed below in the part Results and discussion where the novel parts are recognized by the absence of references to literature. The results of this study bring more insight into the transition between the stripe and the slab confining geometry and

might be advantageous for experimental measurements of DNA elongation in nanochannels of various geometries.
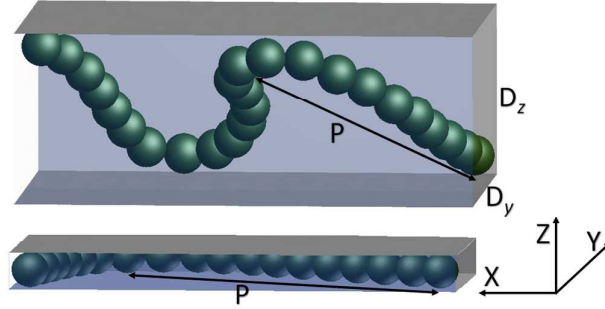
Fig. 1 Fragment of a chain confined to a channel in the form of a slab (upper snapshot) and a stripe (lower snapshot).

I.   Simulation method

For the simulations of a semiflexible polymer chain the bead-spring worm-like chain (WLC) model was used. This model has been already satisfactorily adopted in previous studies of a chain confined in a channel.[17,37] The discretized version of the WLC model consists of N effective monomers (beads) connected by fluctuating effective bonds (springs) characterized by the spring constant. The total potential energy of a chain consisted of a contribution due to the bond stretching, bending of two consecutive effective bonds and of nonbonded pair interactions between the effective monomers. For the bonded and nonboded pair interactions between monomers the established model was used.[38] The effective bonds were described by the FENE (finitely extensible nonlinear elastic) potential

$$\frac{U_{\text{FENE}}(l)}{k_{\text{B}}T} = -\kappa(l_{\text{max}} - l_{\text{o}})^2 \ln\left[1 - \left(\frac{l - l_{\text{o}}}{l_{max} - l_{o}}\right)^2\right] \tag{4}$$

The stretching of bonds was assumed temperature independent with the spring constant $\kappa = 20$ and the maximal allowable bond distance was $l_{\max} = 1$, which serves as a length unit here. The bond lengths varied around the preferred $l_o = 0.7$ with the amplitude $l_{\max} - l_o = 0.3$. The non-bonded interactions were modeled by the shifted and cut Morse potential

$$U_{\mathrm{Morse}}(r) = \varepsilon \left\{ \exp[-2\alpha(r - r_{min})] - 2\exp[-\alpha(r - r_{min})] + 1 \right\} \qquad (5)$$

for $r < r_{\min}$ and zero otherwise, ε was set to 1 k_BT while the distance at the minimum and the steepness of the potential energy function was set to $r_{min} = 0.8$ and $\alpha = 24$, respectively. Such a combination of parameters gives the bead core radius close to $w/2 = 0.38$. Considering the spherical shape of effective monomers, since the width w of a chain slightly exceeded the effective bond length $<l> \approx l_o$ the employed model was from the category of partially fused-spheres approaches. There were negligible nonbonded interactions between monomers separated by more than $l_{\max}$.

The variation of the chain stiffness was modeled by the bending potential between two consecutive bonds in the polymer chain[39]

$$U_{\mathrm{bending}}(\gamma) = b^*(1 + \cos\theta) \qquad (6)$$

where θ was the valence angle between two consecutive effective bonds in the chain, and b^* denoted the bending parameter, which quantified the chain rigidity and entered eqn (6) in units of interaction energy parameter ε. Since the bending was regarded as temperature dependent the actual stiffness of the chain backbone was characterized through the bending parameter $b = b^*/k_BT$. For the discretized WLC model the bending parameter b was related to the persistence length as $b = P/a$ with the monomer size $a = w = l_o$.[40] In the simulations the bending parameter was set to $b = 10$. A prominent example in this study and frequently referred example is a DNA macromolecule. The focus here, however, is on semiflexible

macromolecules generally. Although, the commonly accepted bending parameter for double-stranded DNA under high ionic strength conditions is 50 nm, corresponding to $b = 20$ in the present simulations and $a = 2.5$ nm, the lower bending parameter $b = 10$ allowed to increase the number of Kuhn segments in a chain. Such a choice was also used in deciphering DNA organization in viral capsids.[41] In the present work, the chain length was set to $N = 2000$ effective monomers, the persistence length was $P/a = 9.97$ for a free unconfined chain, corresponding to $L/P = 200.6$. Persistence length P was evaluated from the bond orientation correlations along the free chain at short distances of the order of single persistence length along the chain contour, $\langle \cos \theta_{i,j} \rangle = \exp\left[-\frac{a|i-j|}{P}\right]$, where this relation holds quantitatively in contrast to the behavior at longer distances.[42] The simulations were performed at the constant reduced temperature $T^* = k_B T/\varepsilon = 1$ which corresponds to the good-solvent conditions for a given model.

The walls of the confinement in a slab and a slit were modeled using hard-wall potential. The bead centers were not allowed to move beyond the width D' and the real confinement corrected for chain thickness was given as $D = D' + w$ in accord with previous works.[43-45] The periodic boundary conditions were applied along the long channel axis aligned with the x coordinate.

Our systems of confined chains are schematically shown in Fig. 1. Throughout this paper, the slab is termed a rectangular channel with sides $D_y \times D_z$, both larger than the monomer size and a stripe is termed a rectangular channel with one side $D_z << D_y$ of the order of the monomer size. In order to investigate the effect and interplay between different stripe ($D_z/P = 0.194$) and slab (in the range of $D_z/P = 0.679, 1.535, 2.961, 5.813$) geometries and chain regime appearance, simulation runs were performed for 16 different parameters of D_y in the range of $D_y/P = 0.394 – 11.52$. To validate the chain extension dependence as a function

of the persistence length, the simulations were performed also for 11 different bending

parameters in the range of $b = 0 - 35$ for a chain in a channel $D_y = D_z = D$ of cross-section

$D/P \times D/P = 1.535 \times 1.535$. The initial conformation was a completely straight chain aligned

with the channel axis. The Monte Carlo (MC) simulations were performed using Metropolis

method, which included chain updates by reptation and small random bead displacements

with the amplitude of $0.125 l_o$. To analyze chain behavior and average sample properties

10^7 MC steps (including $\sim 10^{10}$ conformation updates, in each of which one reptation move

was combined with 10 bead displacements) were computed. Analyzing the end-to-end

distance autocorrelation functions we estimated that the overall simulations extended over

300 to 1200 coil relaxation times at different confinements. Here, however, we did not

analyze the reported dependence of relaxation times on confinement.[2,46] The influence of the

confinement was also reflected on the changes of acceptance ratio of moves during the

simulation which decreases approximately to one third on going from the widest slab

investigated to narrow stripes. The resulting thermodynamic averages formed smooth curves

and the errors of data are typically of the respective marker sizes.

II.   Results and discussion

For strong confinement the chain extension along a channel as a result of confinement

in two directions y and z is given by eqn (2). However, here we concentrate on a moderate

confinement where the situation is more complex for semiflexible chains and where most of

linearization experiments are performed. For weak or moderate confinement the scaling

analysis of the chain extension R along the channel with the geometry of a two dimensional

stripe (or a classical $3d$ channel) is based on the linear arrangement of blobs[35] in a channel of

the width D equal to the blob size, $R \approx (N/g)D$. Here, the arrangement of g segments in each

blob depends on the regime of a coil determined by D and is given as $D \sim g^v$, where the exponent v is defined according to the Flory theory as $v = 3/(d+2)$ for an excluded volume chain. A chain with the weak excluded volume interactions between monomers behaves as a pseudoideal (theta) chain with $v = 2/(d+1)$, determined by remaining EV from ternary interactions,[47] rather than as an ideal chain with the exponent $v = 1/2$. A realistic pseudoideal chain (with a finite backbone thickness) under confinement differs from an ideal chain and slightly expands in comparison to a free pseudoideal chain that has a size of an ideal coil.[48] The difference between the pseudoideal and ideal states should be considered especially in confined systems. This is because for an ideal chain the extension R along a channel does not depend on D since the ideal chain does not change its size along the unrestricted directions.[48] On the other hand a chain even with weak excluded volume interactions expands along the channel due to the confinement. This is accounted for in the blob analysis where the blobs in a channel are self-avoiding even if the chain fragments within the blobs are pseudoideal.

Together, the blob analysis using the above relations leads to the extension $R \approx L(a/D)^n$, where $L = Na$ is the chain contour length, and to the general eqn (3) for a chain with strong EV interactions. For example, the corresponding exponent for a chain with EV interactions in a stripe[27] is $n = 1/3$. If the excluded volume interactions in a channel- and stripe-confined semiflexible chain are weak we can furnish a general analogy to strong or moderate excluded volume interactions given by eqn (3). Thus in the case of pseudoideal state for a channel ($d = 3$) or for a stripe ($d = 2$) one arrives at

$$R \approx L \left(\frac{a}{D}\right)^{\frac{d-1}{2}} \left(\frac{P}{a}\right) \tag{7}$$

In eqn (7), the size $D \approx ag^{2/(d+1)}(P/a)^{2/(d+1)}$ of a blob containing a chain fragment of g monomers with the screened EV interactions was used. Resulting chain extension relation

$R \approx LP/D$ applies well in a $3d$ channel where not ultimately long semiflexible chains are reported to lack the excluded volume to a high extent and exhibit the pseudoideal behavior.[18,20,23] The exponent n for a stripe-confined chain increases thus from 1/3 for an excluded volume chain to 1/2 for a pseudoideal chain in eqn (3). However, it has been shown that the pseudoideal regime and similarly the extended de Gennes regime are absent in a stripe and the behavior is governed by eqn (3) instead.[27]

For macromolecules with the semiflexible backbone such as DNA confined to a $3d$ channel the pseudoideal transition regime also called the Gaussian de Gennes regime is developed between the extended de Gennes and Odijk regime.[17,18,20,23,49] In this regime, the pseudoideal behavior of a confined chain dictates its conformation which is rich in typical back-folded chain fragments the so-called hairpin substructures.[17] The extension of a semiflexible chain confined in a slit, slab and stripe is compared with the size of a free chain in both the excluded volume regime and the pseudoideal regime in Tab. 1.

Slit confinement. In the case of a slab confinement the situation is somewhat different from a channel. Before concentrating on a slab it is instructive to remind the situation in a slit because features of a slit are present in the slab confinement. It was shown from the investigation of the structure factor of a chain in a slit that in a slit a combined $3d/2d$ behavior is observed on different length scales.[32] Since a slab combines the channel and slit geometry we can expect a combination of $3d/2d/1d$ behavior on different length scales which is analyzed in the further section devoted to the structure factor of a confined chain. According to the scaling and blob theory the extension in a slit can be described as $R_{\text{slit}} \approx (N/g)^y D$, where the exponent describing the arrangement of blobs along the slit walls is $y = 3/4$ for an excluded volume chain and 2/3 for a pseudoideal chain. Using the excluded volume behavior in a blob,[36] $D \approx ag^{3/5}(P/a)^{1/5}$, and $y = 3/4$ we obtain the extension of a chain as

$R_{\text{slit}} \approx aN^{3/4}(P/D)^{1/4}$ for a semiflexible excluded volume chain in a slit, where the scaling

exponent for D has been already reported.[29] For a pseudoideal chain in a slit using $y = 2/3$ and

the pseudoideal chain behavior in each blob, $D \approx (gaP)^{1/2}$, one obtains the extension

$R_{\text{slit}} \approx aN^{2/3}(P/a)^{2/3}(a/D)^{1/3}$ (Tab. 1).

Slab confinement. Upon going from a slit or a channel to a slab the complexity raises

since now, the cross-section is characterized by two dimensions, D_y and D_z, instead of a single

variable D. A direct scaling analysis can describe the behavior of the conformation of a

semiflexible chain in such a slab. This chain can be composed of small excluded volume

blobs of the size $D_z \approx ag_z^{3/5}(P/a)^{1/5}D_z$ being the smaller slab size. These blobs behave as g_z

fragments of a free EV chain and form larger two-dimensional blobs each one of g_y segments

and of the size of a larger slab profile dimension, $D_y \approx (g_y/g_z)^{3/4}D_z$. The larger blobs in turn

are arranged linearly as self-avoiding blobs along the longest x-direction of the slab and thus

analogously to a channel $R_{\text{slab}} \approx (N/g_y)D_y$. Together, when substituting for g_y and g_z, this

double blob analysis leads to the total chain extension

$$R_{\text{slab}} \approx L(aP/D_yD_z)^{1/3} \tag{8}$$

That is an analogy of the chain extension in a channel, $R \approx L(a/D)^{2/3}(P/a)^{1/3}$, or generally of

eqn (3) for variable dimensions and can be obtained also from the original Flory theory.[50]

Such a split of the confinement into two directions was indicated already by Turban.[51] If the

aspect ratio of the channel profile is not unity the single D should be replaced by an average

$D_{\text{av}} = (D_yD_z)^{1/2}$. The split of a chain into $2d$ and $3d$ blobs as described above is affected by an

aspect ratio of the two sizes. Recently, the mixed regime similar to the above double blob

analysis was reported in a channel of variable aspect ratio of rectangular profile by Dorfman

et al.[25]

The extension of a pseudoideal chain in the same slab is obtained as above but using two-dimensional blobs of the size $D_y \approx (g_y/g_z)^{2/3} D_z$ containing pseudoideally organized blobs of the size $D_z \approx (a g_z P)^{1/2}$. The latter blobs are built up of three-dimensional pseudo ideal arrangement of g_z monomers. This leads to the extension

$$R_{\text{slab}} \approx L(P^2/D_y D_z)^{1/2} \tag{9}$$

which is an analogy to eqn (7) if the confinement is symmetric and one takes $D_y = D_z = D$. Interestingly, holding D_z constant and varying only D_y provides the same scaling of the chain extension induced by a slab as the extension induced by a stripe when varying its width D, *i.e.* $n = 1/3$ and $1/2$ for the excluded and pseudoideal behavior, eqns (3) and (7), respectively. Results of our simulations of the chain extension in a stripe and in a slit-like channel (or slab) over a broad range of D_y/P covering the strong and moderate confinements for four thicknesses D_z/P are depicted in Fig. 2. One can recognize the stronger chain extension in a stripe relative to that in a slab and a more significant decrease of the extension on widening the slab. The shorter chain expansion in a slab than in a stripe is in agreement with Tab. 1 where one can notice that the slab induced extension is in fact equal to the stripe induced extension multiplied by a factor of $(a/D_z)^{1/3} < 1$. The Odijk prediction fits the results in the strong confinement, $D_y/P < 1$, only for the two narrowest slabs, with $D_z/P < 1$, namely for $D_z/P = 0.194$ and 0.679. The narrowest slab at $D_z/P = 0.194$, with the slab thickness $D_z/a = 1.93$ does not allow to place two beads in the perpendicular direction to the slab plane and is very close to the stripe geometry. The predicted slope $1/3$ according to eqn (3) shown for a stripe in Fig. 2 is close to this curve and the difference (we observe 0.379 instead of $1/3$) indicates remaining contributions of ideality arising from weakened $3d$ character of the confined chain.
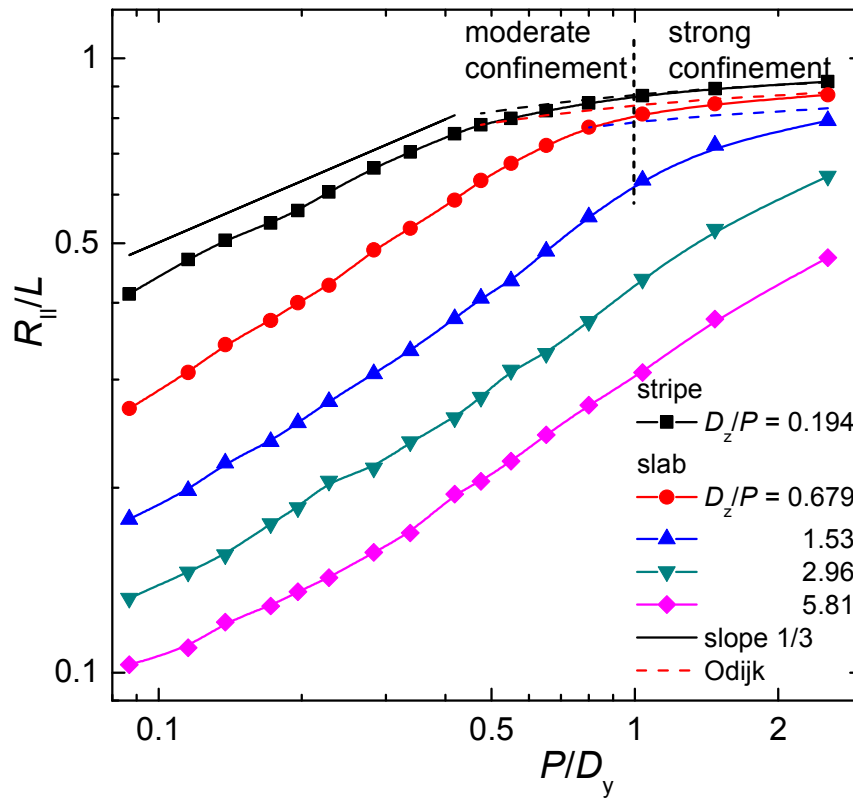
Fig. 2 Transition curves of the reduced chain extension as a function of the reduced

confinement strength over the moderate and strong confinement for a chain of the persistence

length P in a stripe and slab of width D_y and of the four slab thicknesses D_z/P as indicated in

legend.
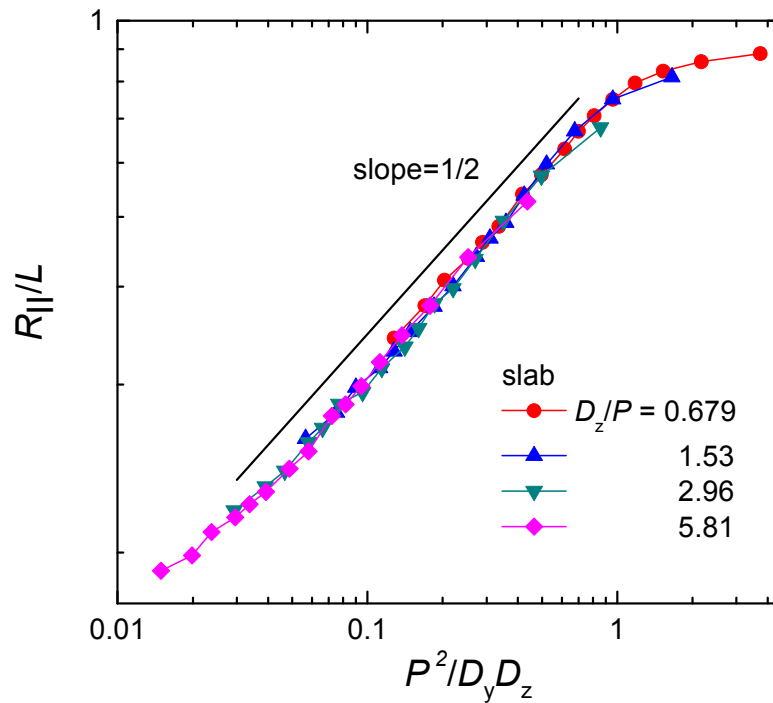
Fig. 3 Master curves of the reduced extension for a chain in a slab of the four slab thicknesses D_z/P and data presented in the previous figure. The slope indicates a pseudoideal behavior according to eqn (9).

Common master curve for a slab presented in Fig. 3 over the range of moderate confinement supports the blob analysis by eqns (8) and (9). At the same time this smooth common curve for different confinement strength indicates sufficient sampling in the simulations. It should be mentioned here that the chain topology (including entanglement, formation of knots or backfolding) and its metric relationship is relevant issue in confined polymers which becomes frequently addressed in recent studies.[29,30,52] Although, we are aware that confinement enhances the knotting probability of a confined chain in comparison to a free chain, we focus here on the overall extension of a chain in a channel assuming excluded volume effects without chain crossings. Thus entanglement and knotting are

possible but not promoted or studied specifically as for instance in a topology-unrestricted

ensemble. Confinement affects also chain dynamic properties. The chain relaxation slows

down with the confinement.[28,31] Aware of this effect, we have performed extensive

simulations to attain the equilibrium properties. One of indications of reaching equilibrium is

the master plot in, Fig. 3, where the data for different confinement obey the same scaling law.

We investigated also the distribution of end-to-end distance and distribution of radius of

gyration of confined chains (not show) that exhibit smooth curves. This again indicates

sufficient sampling and averaging of different possible topological events during long

simulation.

The observed slope close to 1/2 instead of 1/3 reflects the pseudoideal chain behavior,

notice eqn (9) for a pseudoideal chain in a slab above, and represents the slope 1 for single D

of a channel in eqn (7). This is an indication that with the chain lengths here we are still not in

the excluded volume regime. This will be seen further in the structural analysis. The

difference in the slopes between the excluded volume behavior and the ideal chain behavior

can also be seen considering flexible chains, where EV operates, instead of semiflexible

chains, where EV is negligible for not very long chains. Though we tested here such a change

in the slab, this behavior was shown already under the cylindrical channel confinement[18] and

thus it is not presented here. It indicates, however, that the source of deviation in the slope

comes from the presence or absence of EV. Universal curve is designed for the blob regime

and the curves start to deviate on entering the Odijk regime. Data for the two widest slabs,

$D_z/P = 2.961$ and 5.813 for wide D_y also, are already relatively close to the chain in a free

solution, where the extension becomes independent on the confinement, and thus start also to

deviate from the blob scaling. The curve for a stripe does not follow the master curve for a

slab, it is close to the slope 1/3, and is shown only in the previous graph in Fig. 2.

Another indication of the pseudoideal chain behavior can be achieved following the chain extension in a slab as a function of the persistence length P instead of following the dependence on the confinement D since different exponents are predicted in eqn (8) and eqn (9) for this function for an excluded volume chain and for a pseudoideal chain. We focused on this extension in a square channel of moderate confinement strength, $D_z/P = D_y/P = 1.535$, and found that the extension is linearly proportional to P according to eqn (9), as shown in Fig. 4. This further supports the previously discussed pseudoideality in chains that was based on the variations of the extension with the confinement D.
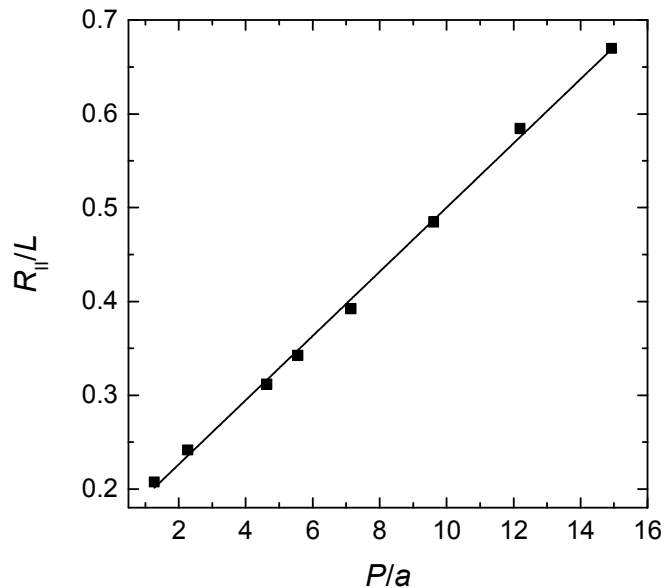
Fig. 4 Relative chain extension of a chain along a channel as a function of the chain persistence length P/a.

An overview of the chain extension in a stripe, slab, channel and a free chain in the regimes involving the excluded volume behavior as well as the pseudoideal behavior from the previous discussion is presented in Tab. 1. Here, only one EV regime is included because the

de Gennes blob regime and the extended de Gennes regime are not differentiated in the chain extension.[10]

Tab. 1 The extension of a semiflexible chain confined in a slit, slab and stripe in the excluded volume and pseudoideal transition regimes. The size of an unconfined chain is also included for comparison.

		Excluded volume regime		Pseudoideal regime	
free chain		$N^{\frac{3}{d+2}} a \left(\frac{P}{a}\right)^{\frac{1}{d+2}}$		$N^{\frac{2}{d+1}} a \left(\frac{P}{a}\right)^{\frac{2}{d+1}}$	
slit		$N^{\frac{3}{4}} a \left(\frac{P}{D}\right)^{\frac{1}{4}}$		$N^{\frac{2}{3}} a \left(\frac{P}{a}\right)^{\frac{2}{3}} \left(\frac{a}{D}\right)^{\frac{1}{3}}$	
channel $d=3$	slab $d=3$	$Na \left(\frac{P}{a}\right)^{\frac{1}{3}} \left(\frac{a}{D}\right)^{\frac{d-1}{3}}$	$Na \left(\frac{P}{a}\right)^{\frac{1}{3}} \left(\frac{a^2}{D_y D_z}\right)^{\frac{1}{3}}$	$NP \left(\frac{a}{D}\right)^{\frac{d-1}{2}}$	$NP \left(\frac{a^2}{D_y D_z}\right)^{\frac{1}{2}}$
	stripe $d=2$		$Na \left(\frac{P}{D}\right)^{\frac{1}{3}}$		$NP \left(\frac{a}{D}\right)^{\frac{1}{2}}$

One should notice the limits of application of the tabulated expressions. For this purpose we use the original Flory approach for a confined chain[50] which produces the same relations for the chain extension as the renormalized Flory approach.[16] The Flory expression for the free energy of a semiflexible chain in the slab geometry reads

$$\frac{F}{k_B T} \approx \frac{R^2}{R_o^2} + \left(\frac{N}{N_P}\right)^2 \frac{aP^2}{R D_y D_z} \tag{10}$$

where $R_o^2 = 2NaP$ in the first, elasticity term is the squared size of an ideal semiflexible chain and $N_P = P/a$ and aP^2, respectively, are the number of monomers in one persistence length and the excluded volume in the second, interaction term. The minimization with respect to R leads to eqn (8) for the chain extension R in a slab. This is, however, a very general approach and replacing the volume term RD_yD_z in the denominator of the second interaction term with R^3 equation applies as well for a free chain in three-dimensional space. Similarly, replacement with RD^2, R^2D and aRD and subsequent minimization provides the chain extension relation for a cylindrical channel, slit and stripe, respectively, as presented in Tab. 1. The border between the ideal and excluded volume regime can be discerned from the interaction term of these equations. If this term becomes larger than unity the excluded volume regime sets in. When we start from a free chain and consider the interaction term for the unperturbed state $(R = R_o)$ to be larger than unity we obtain the onset of the EV regime for a free chain which also corresponds to the onset D^* of the classical de Gennes regime for a geometrically confined chain. Therefore a free chain of $N^* > (P/a)^{d/(4-d)}$ monomers is long enough for the EV effects to operate. Notice here that more significant EV effects set in for shorter chains when $d = 2$ ($N^* > P/a$) than for $d = 3$ ($N^* > (P/a)^3$). At the same time, this limit of N^* monomers defines the size of a thermal blob,[53] $\xi_T \approx (N^*aP)^{1/2} \approx aN^{*3/5}(P/a)^{1/5}$, which is in fact equivalent to the onset of the classical de Gennes regime with $D^* \approx \xi_T \approx a(P/a)^{2/(4-d)}$ for a geometrically confined chain. This is obtained if the above limit for a free chain of N^* is used in the size expression for an ideal blob of the channel diameter $D^* = (N^*aP)^{1/2}$. For the channel geometry we recover $D^* > (P^2/a)$.

On decrease of the channel dimension D below the limit for the classical de Gennes regime, $P < D < a(P/a)^{2/(4-d)}$, the statistics within a blob transforms from the EV statistics into an ideal statistics and we have a coexistence of these two statistics. This regime is termed as

the extended de Gennes regime in the literature.[20,27] Now, the total chain extension is obtained

as a linear array of self-avoiding anisometric blobs (ellipsoids in the case of a $3d$ channel and

ellipses in the case of a $2d$ channel) of transverse lengths D or D_y and D_z for the more general

case of the slab geometry and longitudinal length H.[49] The coexistence of both types of

behavior requires that the number of monomers g in an anisometric blob is obtained assuming

the interaction term in the particular Flory expressions for the free energy being set to unity,

i.e. $g^2 a^d/(HD^{d-1}) \approx 1$ for a cylindrical channel or for a stripe and $g^2 a^3/(HD_y D_z) \approx 1$ for a slab

together with $H \approx (gaP)^{1/2}$. This yields $g \approx (D/a)^{2(d-1)/3}(P/a)^{1/3}$, which is $D^{4/3}P^{1/3}/a^{5/3}$ for a

cylindrical channel[10] and $(D_y D_z)^{2/3}P^{1/3}/a^{5/3}$ for a slab. For a channel these assumptions yield

$H \approx a(P/a)^{2/3}(D/a)^{(d-1)/3}$. The linear arrangement of such blobs $R \approx (N/g)H$ provides the chain

extension dependence identical with eqn (3). As mentioned already both regimes provide

indistinguishable chain extension relations. Moreover, it has been pointed out that the

transition between the classic and extended de Gennes regime is continuous, *i.e.* both

extension relations contain the same numerical prefactor.[20] Further decrease of D close to

$D \sim P$ leads to a transition regime where chains behave as ideal or pseudoideal and extension

was described by relation $R \sim NP/D$.[18,20,23] Appearance of these three particular blob regimes

depends on the set of parameters (D, N, P, a) and not all regimes will appear necessarily in

the system, which is also the case here. Ultimately, under a strong confinement, $D < P$, the

deflection regime of Odijk sets in.

Once we have the limits of applications of the above relations in Tab. 1 we can make

contact with our data. According to the Flory theory,[50] the classical de Gennes regime is

expected for a free chain of $N^* > (P/a)^3 \approx 1000$ segments here (only 2 spherical blobs), in a

channel ($3d$) with the diameter of side length $D^*/a \approx (P/a)^2 > 99.3$ ($D^*/P \approx P/a > 10$) but for a

chain in a stripe ($2d$) it appears already for $N^* > (P/a) \approx 10$ (200 blobs here) with the width

$D^*/a \approx P/a > 10$ ($D^*/P > 1$). Thus, while for a chain of $N = 2000$ segments confined to a

channel used here the classical de Gennes regime can hardly occur it is not true for this chain in a stripe. Concerning the potential extended de Gennes regime to be observed, several anisometric blobs of a chain confined in a slab or cylindrical channel should be formed. For instance, in a cylindrical channel of $D/P = 1.53$ a chain is supposed to form about $N/(D^{4/3}P^{1/3}/a^{5/3}) \approx 24$ blobs while in a slab-like channel of $D_y/P = 11.54$ and $D_z/P = 1.53$ this number drops to about $N/(D_y^{2/3}D_z^{2/3}P^{1/3}/a^{5/3}) \approx 6$ blobs. From the presented simulations it turns out that neither the classical nor extended de Gennes regime has been achieved in the slab-like confinement. Instead, the pseudoideal behavior has been observed in a slab. On the contrary, the simulation results here for the stripe-like confinement support the conclusions due to Huang and Bhattacharya[27] on prevailing EV behavior in a stripe. The pseudoideal regime has not been observed for this geometry even for semiflexible chains which have tendency to exhibit the ideal behavior.

From the relations for the slab and stripe presented in Tab. 1 it is clear that from the R vs D_y behavior at constant D_z one cannot differentiate between the stripe and the slab. In both regimes the scaling of the chain extension is the same: either $D_y^{-1/3}$ ($D^{-1/3}$) for the excluded volume regime or $D_y^{-1/2}$ ($D^{-1/2}$) for the pseudoideal regime. However, since the regimes are changed here when going from the stripe to the slab one can establish an estimate of the border where the stripe character turns into that of the slab confinement. The first transition curve, when making this change in Fig. 2, for $D_z/P = 0.194$, which is considered to be a stripe bears already the sign of the behavior in a slab.

It should be mentioned that in order to compare to the published data for a stripe,[27] we have used here similar chain lengths also for the slab. There is a need, however, to use also longer chains in simulation which would enable to follow also the non-gaussian regimes in a

slab.[24] The situation described here should be typical for the experimental range with α-DNA

or T4-DNA macromolecules.[23,54]

 Structure factor. Compared to the original paper of Huang and Bhattacharya[27] we

want to point out a new aspect and thus supplement their study. That is why we opted for the

structure factor which reflects the properties of confined chain on different scales. The

arrangement of chain segments on different length scales is well reflected on the single chain

structure factor defined for an isotropic chain as

$$S(q) = \frac{1}{N^2} \langle \sum_{i=1}^{N} \sum_{j=1}^{N} \sin(qr_{ij})/qr_{ij} \rangle \qquad (11)$$

where r_{ij} is the distance between segments i and j and the wavevector $q = 2\pi/x$ covered the

range of size values x varying from the monomer size to about the chain size. The structure

factor provides complementary information to that gained from the chain extension *vs.*

confinement strength dependence. In a logarithmic scale of the structure factor one can

recognize different regions characterized by different slopes since $S(q) \sim q^{-1/v}$ where v is the

scaling exponent in the $R \sim N^v$ relation. Finally, in the Guinier regime,[55] *i.e.* for $q < 2\pi/R$, the

structure factor saturates. The values of the slopes are governed by the regime of the chain

conformation as well as by the length scale and are presented for a free and geometrically

confined chain in the excluded volume and pseudoideal regime in Tab. 2. As can be seen at

sufficiently large wavevectors $q > 2\pi/P$ the particular fragment of a chain is viewed as a rigid

rod and for semiflexible chains this local conformation, characterized by slope −1, is always

present in the $S(q)$ plots (Fig. 5). Upon going from larger to smaller values of the wavevector,

which corresponds to going from smaller local to larger global length scales, the rod-like

behavior transforms into a two- or three-dimensional behavior. It also follows from Tab. 2

that the most complex behavior might be expected in the $S(q)$ plot of a chain confined in a

slab where up to 4 regions of different slopes might be recognized. Notice, however, that for

complete observation of all regions and applicability of the above discussed hierarchical blob

analysis such criteria as the sufficient length of a chain and $P < D_z < D_y$ have to be met.

As seen in Fig. 5, which is focused on the limiting cases, the structure factor plotted in

logarithmic scale for a chain confined in the stripe-like geometry with the aspect ratio

$D_y/D_z = 45.9$ ($D_z/P = 0.251$, $D_y/P = 11.5$) displays a region with slope −4/3. This indicates the

two-dimensional conformation of the self-avoiding blobs. While the latter finding has already

been drawn from Fig. 2, the planar arrangement follows exclusively from Fig. 5. As the

aspect ratio D_y/D_z decreases the region of the slope −4/3 gradually ceases till it diminishes as

can be seen in Fig. 5 for a chain in narrow slab (channel) with the aspect ratio $D_y/D_z = 1.57$

($D_z/P = 0.251$, $D_y/P = 0.394$) and with the slope –1 over all scales. The logarithmic plots of

$S(q)$ for a chain confined in slabs with $(D_y D_z)^{1/2}/P < 1$ decreases with the slope –1 virtually

over the all investigated q interval.

In the next figure we want to address all possible regions characterizing different

length scales. As Fig. 6 shows, the linear arrangement of blobs which is reflected on the slope

−1 at small wavevectors is seen in all channels and is best recognizable for the narrow

channel. The intermediate interval of wavevectors reflects the organization of segments at

length scales comparable to the channel dimensions. The slopes expected in these regions are

also indicated. In Fig. 6, the slope −4/3 fits the $S(q)$ plot for a chain in the slab of

$D_y/P = 0.394$ (aspect ratio 14.8, notice that in this particular case $D_y < D_z$) until $q \approx 0.08$ when

a chain is viewed more as a linear array of blobs. In this slab the chain conformation is thus

still governed more by the excluded volume (slope −4/3) than by the pseudoideal statistics

(slope −3/2).

However, in agreement with the findings based on the analysis of the chain extension behavior in the confinement, the investigation of all structure factors reveals that there is no region characterized by the slope $-5/3$ which would indicate an existence of the length scale within a chain where the EV statistics of a three-dimensional coil dominates. Instead, the region with the slope closer to -2 commences in logarithmic plots of $S(q)$ for a chain in channels (slabs) of D/P (D_y/P, D_z/P) ≥ 1.535 (Fig. 6) as the wavevector drops below $2\pi/P$. This can indicate the chain conformation induced by a channel or slab within an anisometric blob in the extended de Gennes regime or within a spherical blob in the pseudoideal regime (Tab. 2). Here, we can benefit from the complementarity with the chain extension dependence. As the variation of the chain extension with the confinement strength shows (Figs. 2, 3) this rather indicates the statistics of a pseudoideal fragment in a spherical blob. Nevertheless, the expected slope $-3/2$ characteristic for two-dimensional organization of segments in the pseudoideal regime does not fit any plot in the intermediate region. This is most likely attributable to the small aspect ratio of the channel cross-sections.
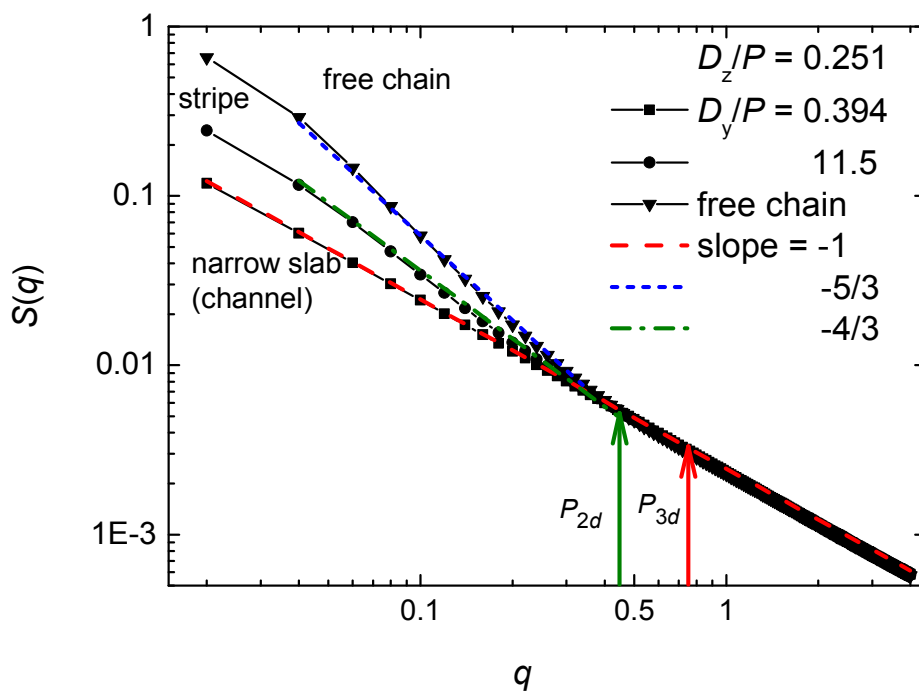
Fig. 5 Logarithmic plot of the structure factor $S(q)$ for a chain confined in a stripe, in a narrow slab (channel) and for a free chain. Lines parallel to the plots depict the slopes for a rod-like chain (-1), for a free three-dimensional excluded-volume coil ($-5/3$) and for a chain in a stripe reflecting the two-dimensional excluded volume behavior ($-4/3$). Arrows show the positions of two-dimensional and three-dimensional persistence lengths P_{2d}, P_{3d}, respectively.

24
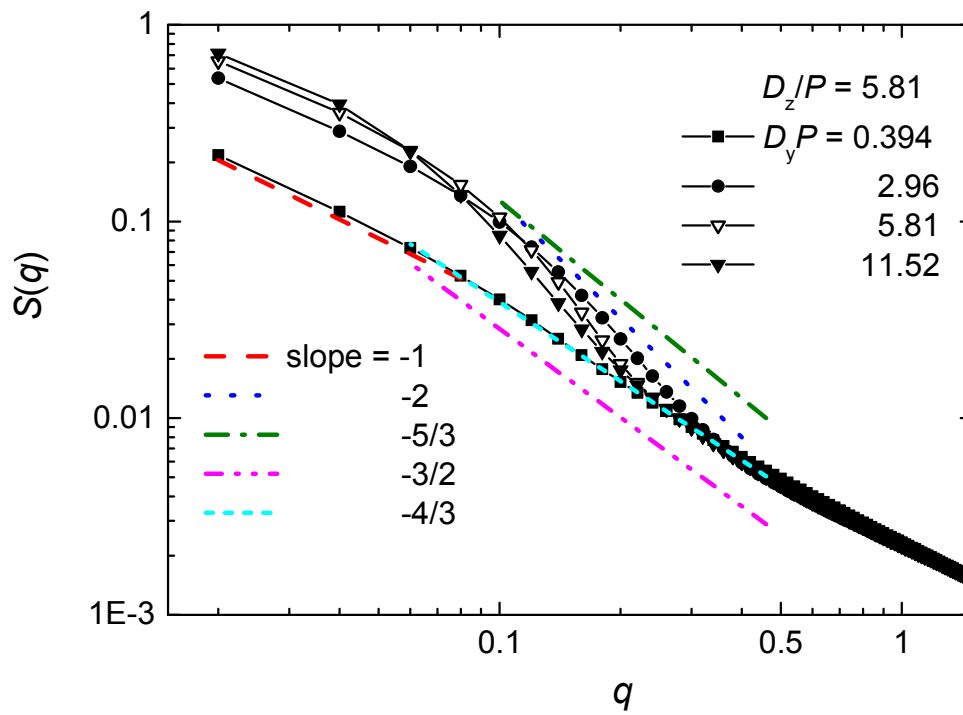
Fig. 6 Logarithmic plot of the structure factor for a chain confined in the slab geometry specified in the legend. The slopes indicating the chain extension scaling with the chain length are guides for the eye.

Tab. 2 Predicted values of the slopes $1/v$ (in bold) for the structure factor $S(q) \sim q^{-1/v}$ dependence in a logarithmic scale for a free semiflexible chain and for a chain in different geometrical confinements and regimes. The predicted intervals of the wavevector q characterized by the slopes are also delineated, R holds for the chain size in the direction(s) in which the chain conformation is completely free to relax. The substitution $q' = q/2\pi$ is used for brevity.

		Excluded volume regime			Pseudoideal regime		
free chain	$d = 3$	$q' > 1/P$ **1** $1/P > q' > 1/R$ **5/3**			$q' > 1/P$ **1** $1/P > q' > 1/R$ **2**		
	$d = 2$	$q' > 1/P$ **1** $1/P > q' > 1/R$ **4/3**			$q' > 1/P$ **1** $1/P > q' > 1/R$ **3/2**		
slit		$q' > 1/P$ **1** $1/P > q' > 1/D$ **5/3** $1/D > q' > 1/R$ **4/3**			$q' > 1/P$ **1** $1/P > q' > 1/D$ **2** $1/D > q' > 1/R$ **3/2**		
channel $d = 3$	slab^c $d = 3$	$q' > 1/P$ **1** $1/P > q' > 1/D$ **5/3^a; 2^b** $1/D > q' > 1/R$ **1**	$q' > 1/P$ **1** $1/P > q' > 1/D_z$ **5/3^a; 2^b** $1/D_z > q' > 1/D_y$ **4/3** $1/D_y > q' > 1/R$ **1**		$q' > 1/P$ **1** $1/P > q' > 1/D$ **2** $1/D > q' > 1/R$ **1**	$q' > 1/P$ **1** $1/P > q' > 1/D_z$ **2** $1/D_z > q' > 1/D_y$ **3/2** $1/D_y > q' > 1/R$ **1**	
	stripe $d = 2$		$q' > 1/P$ **1** $1/P > q' > 1/D_y$ **4/3** $1/D_y > q' > 1/R$ **1**			$q' > 1/P$ **1** $1/P > q' > 1/D_y$ **3/2** $1/D_y > q' > 1/R$ **1**	

^{a} classical de Gennes regime, ^{b} extended de Gennes regime, ^{c} $D_z < D_y$

Orientation correlations. The organization of a chain in a channel can also be inferred from the tangent-tangent orientation correlation function which is defined along a chain of the

arc length s as $<\cos \theta(s)> \, = \, <\boldsymbol{u}(k)\boldsymbol{u}(k+s)>$ where $\boldsymbol{u}(k)$ is the unit vector at point k along the chain contour and the average is running through the all generated conformations and different positions k. While this function is exponentially decaying for a free WLC chain, the strong confinement ($D \ll P$) induces typical, more complex pattern of the orientation correlations. If the interactions of monomers with the confining channel walls are represented by the harmonic potential the analytic relation for an asymmetric channel reads[56]

$$<\boldsymbol{u}(k)\boldsymbol{u}(k+s)> \, = 1 - \frac{\lambda}{2P}\left[1+\sqrt{2}\exp[-s/\lambda]\sin\left(\frac{s}{\lambda}-\frac{\pi}{4}\right)\right] \qquad (12)$$

According to eqn (12), before the plateau is reached the initial decay of the orientation correlations is followed by a minimum positioned at $s_{min} = \lambda\pi/2$. The characteristic deflection length λ is a function of the chain stiffness and the channel dimensions $\lambda = c(D^2 P)^{1/3}$ where c is a constant of the order of unity.[11] It is thus of interest to examine the applicability of the analytic relation for the channels with asymmetric cross-sections when substituting $D_y D_z$ for D^2, i.e. $\lambda \approx (D_y D_z P)^{1/3}$.

Two fitting procedures to eqn (12) have been adopted for the orientation correlation functions. In one procedure, only c is considered as a fitting parameter while in the second procedure, P is not fixed to its free chain value but is assumed as an additional fitting parameter instead. The orientation correlation functions along with their best one-parameter and two-parameter fitting curves for a strongly confined chain are presented in Fig. 7.

It is obvious that the one-parameter fitting is of worse quality than the two-parameter fitting in agreement with our previous findings.[37] The best fit is obtained for the square channel and the quality of fitting gradually deteriorates with the increasing asymmetry of the channel. The increase of the channel asymmetry is also responsible for the enhanced difference between the one- and two parameter fits. The fits around minimum are not

satisfactory in any case. In comparison with the analytical predictions, the minima are shallower and shifted toward larger contour fragments s. When P parameter is fixed to its material value the one-parameter fitting yields $c = 0.74$ for the square channel, $c = 0.83$ and $c = 0.65$, 0.73 and 0.80 for the stripes of $D_y/P = 0.394$, 0.679 and 0.964, respectively. The two-parameter fitting leads to the following combinations (c, P): $(0.73, 10.2)$, $(0.78, 9.2)$, $(0.69, 8.94)$, $(0.88, 13.2)$ and $(1.00, 14.0)$ for a chain in the square channel, slab and stripes of increasing asymmetry, respectively. It seems that the parameter c in the expression for the deflection length does not behave as a universal constant. Thus it is not surprising that the position of a minimum in the orientation correlations s_{min} does not display the expected scaling $\sim D_y^{1/3}$ as it can be seen in Fig. 8. One can also see that the orientation correlation function does not discern between the stripe and slab geometry.
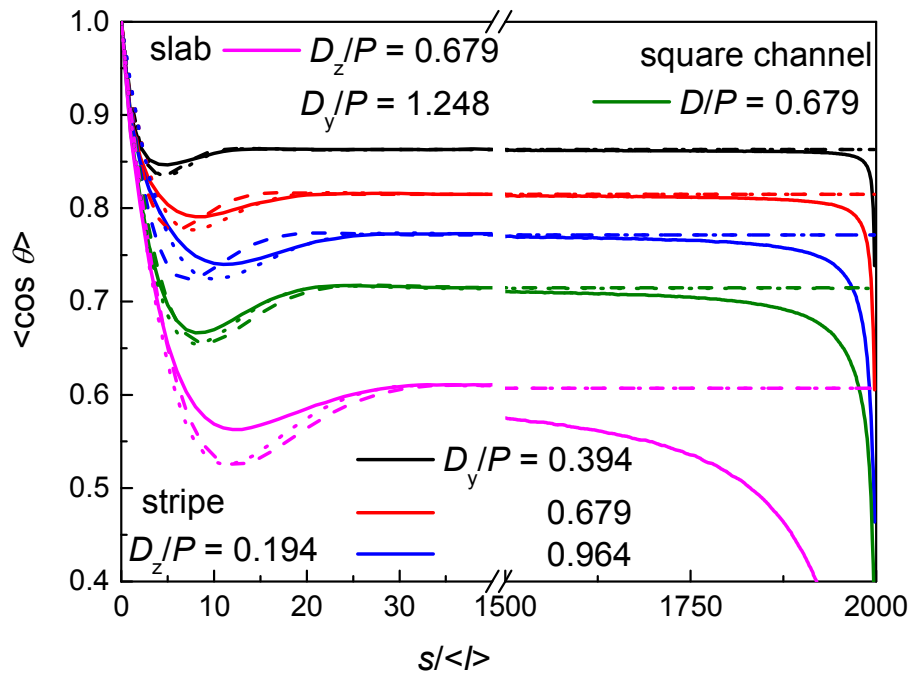
Fig. 7 The orientation correlations for a chain in a stripe, slab and channel with corresponding

one- and two- parameter fits based on eqn (12) shown by dashed and dotted lines,

respectively. The curves are vanishing for $s = 1999$.
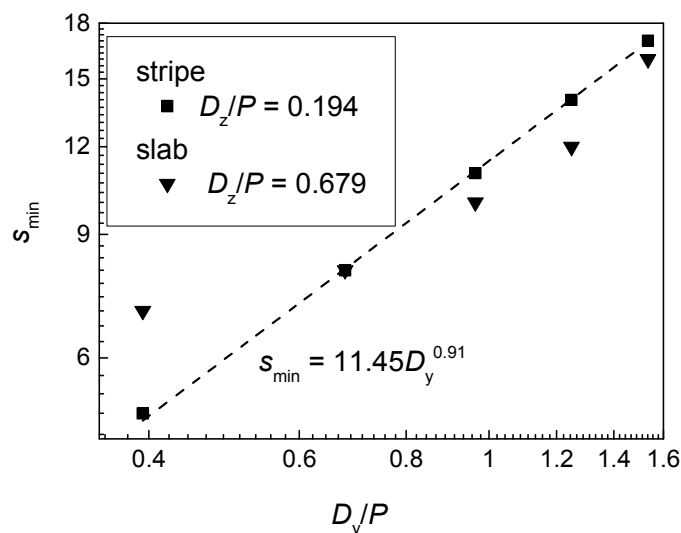
Fig. 8 The position of a minimum s_{min} in the orientation correlations as a function of the

stripe/slab width D_y in a logarithmic scale for a strongly confined chain in a stripe/slab. The

fitting line and corresponding equation are also included for the stripe confinement.

The qualitative behavior of the orientation correlations remains similar for the wider stripes or

slabs beyond the Odijk regime (not shown). The minimum, however, becomes less apparent

and the orientation correlations are diminishing. The presence of hairpin substructures[17] in the

confined chains demonstrates itself in the negative orientation correlations around the shallow

minimum in the case of the slabs with $D_y/P > 1$ and $D_z/P > 1$.

29

III.   Conclusions

Significant chain extension in a stripe which is due to the strong excluded volume interactions between monomers in two dimensions weakens considerably on transition to experimentally feasible slit-like channels. Based on the chain extension-confinement strength dependence and the structure factor behavior for a chain in a stripe we infer the excluded volume regime (classical de Gennes regime) typical for two-dimensional systems. On widening of the stripe in direction perpendicular to the stripe plane, *i.e.* on transition to the slab geometry, the advantageous chain extension decreases and the Gaussian regime is observed for not very long semiflexible chains.

The slab behavior is observed when the two-dimensional stripe (originally of one-monomer thickness) reaches the reduced thickness in the third dimension larger than $D/P \approx 0.2$. This maximum height of the slab to retain the advantage of a stripe is very low and have implications for DNA linearization experiments as in wider slabs the favorable strong extension disappears and the intermediate regimes may appear which complicate the analysis in linearization experiments.

Universality in the evolution of the chain extension with the moderate confinement strength was found. The observed scaling shows the pseudoideal behavior. It should be noted that this situation, where the EV regime is not reached for DNA chains, is observed quite often in experiment. It was shown that α-DNA or T4-DNA macromolecules, used most often in experiments, are in a transition state between the Gaussian and swollen coil regime.[23,54] Earlier experimental and simulation reports often declared Gaussian behavior. Only recently the excluded volume regime has been reached in extensive simulations with longer chains.[24,26] For longer chains except the transition Gaussian regime we would observe also the de Gennes and extended de Gennes excluded volume regimes.

The structure factor of a chain reveals regimes and details of the chain conformation on different length scales and confirm the structural predictions of the blob analysis. The structure factor provides information complementary to and in accord with the behavior of the extension-confinement curves. All four possible regions predicted for the structure factor dependence on the wavevector of a chain confined to a slab (Tab. 2) have not been observed in the presented systems. In summary, in all curves one can notice the rod-like behavior, slope -1, locally at high q as well as globally at small q. For the middle range, in a very thin slab close to a stripe situation, $D_y/P = 0.394$, we observe $2d$ blob organization with the slope $-4/3$. For broader slabs, the blobs are recognized, the $2d$ behavior does not appear anymore and the 3d blobs are leaning more towards the ideal chain behavior with the slope -2 compared to the EV regime with the slope $-5/3$ in accord with the behavior in extension curves. In order to reach and detect all the anticipated regions of behavior in the structure factor one needs a much longer chain entrapped in a slab of significant asymmetry ($D_y \gg D_z$) and enough space for a chain fragment within a blob to coil up.

The evidence for pseudoideality in confined chains is based on four indicators: the extension curves, variation of the extension with the persistence length, estimated limits for the regimes in investigated systems and the structure factor behavior.

The orientation correlation functions for a chain in the stripe and sufficiently narrow slabs display behavior predicted by the analytical theory though with the increasing asymmetry the quality of fitting curves is worsened. From the fitting curves also follows that the numerical constant in the deflection length relation does not seem to be a universal constant but rather a geometry depended parameter.

Acknowledgements

Table of Content graphics
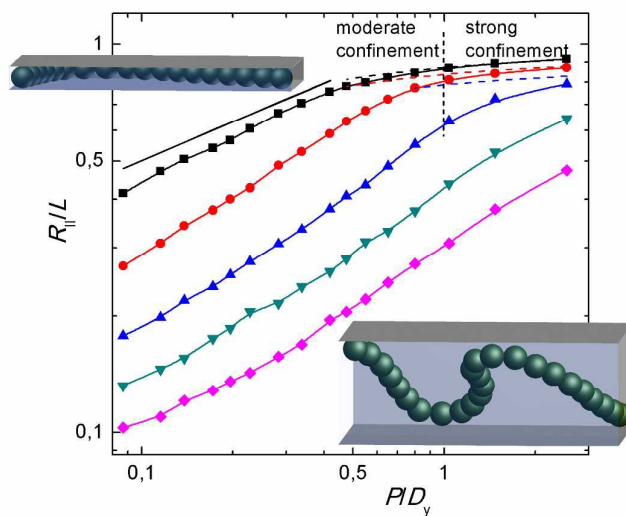
Chain extension along the channel *vs* confinement curves for the stripe-like channel (upper curve) and in four slab-like channels of increasing thickness in the transition curves below.

References

1.   J. O. Tegenfeldt, C. Prinz, H. Cao, S. Chou, W. W. Reisner, R. Riehn, Y. M. Wang, E. C. Cox, J. C. Sturm, P. Silberzan and R. H. Austin, *Proc. Natl. Acad. Sci. U. S. A.*, 2004, **101**, 10979-10983.

2.   W. Reisner, K. J. Morton, R. Riehn, Y. M. Wang, Z. Yu, M. Rosen, J. C. Sturm, S. Y. Chou, E. Frey and R. H. Austin, *Phys. Rev. Lett.*, 2005, **94**, 196101.

3.   C. H. Reccius, J. T. Mannion, J. D. Cross and H. G. Craighead, *Phys. Rev. Lett.*, 2005, **95**, 268101.

4.   M. C. Choi, C. D. Santangelo, O. Pelletier, J. H. Kim, S. Y. Kwon, Z. Wen, Y. Li, P. A. Pincus, C. R. Safinya and M. W. Kim, *Macromolecules*, 2005, **38**, 9882-9884.

5.   K. Jo, D. M. Dhingra, T. Odijk, J. J. de Pablo, M. D. Graham, R. Runnheim, D. Forrest and D. C. Schwartz, *Proc. Natl. Acad. Sci. U. S. A.*, 2007, **104**, 2673–2678.

6.   S. Köster, J. Kierfeld and T. Pfohl, *Eur. Phys. J. E*, 2008, **25**, 439-449.

7.   C.-C. Hsieh and P. S. Doyle, *Korea-Aust. Rheol. J.*, 2008, **20**, 127-142.

8.   Y. Kim, K. S. Kim, K. L. Kounovsky, R. Chang, G. Y. Jung, J. J. de Pablo, K. Jo and D. C. Schwartz, *Lab Chip*, 2011, **11**, 1721-1729.

9.   K. D. Dorfman, S. B. King, D. W. Olson, J. D. P. Thomas and D. R. Tree, *Chem. Rev.*, 2012, **113**, 2584-2667.

10.   W. Reisner, J. N. Pedersen and R. H. Austin, *Rep. Prog. Phys.*, 2012, **75**, 106601.

11.   T. Odijk, *Macromolecules*, 1983, **16**, 1340-1344.

12.   Y. Yang, T. W. Burkhardt and G. Gompper, *Phys. Rev. E*, 2007, **76**, 011804.

13.   J. Kalb and B. Chakraborty, *J. Chem. Phys.*, 2009, **130**, 025103.

14.   T. W. Burkhardt, Y. Yang and G. Gompper, *Phys. Rev. E*, 2010, **82**, 041801.

15.   J. O. Tegenfeldt, C. Prinz, H. Cao, R. L. Huang, R. H. Austin, S. Y. Chou, E. C. Cox and J. C. Sturm, *Anal. Bioanal. Chem.*, 2004, **378**, 1678-1692.

16.   S. Jun, D. Thirumalai and B.-Y. Ha, *Phys. Rev. Lett.*, 2008, **101**, 138101.

17.   P. Cifra, Z. Benková and T. Bleha, *J. Phys. Chem. B*, 2009, **113**, 1843-1851.

18.   P. Cifra, *J. Chem. Phys.*, 2009, **131**, 224903.

19.   P. Cifra, Z. Benková and T. Bleha, *Phys. Chem. Chem. Phys.*, 2010, **12**, 8934-8942.

20.   Y. Wang, D. R. Tree and K. D. Dorfman, *Macromolecules*, 2011, **44**, 6594–6604.

21.   L. Dai, S. Y. Ng, P. S. Doyle and J. R. C. Van der Maarel, *ACS Macro Lett.*, 2012, **1**,
       1046−1050.

22.   J. Z. Y. Chen, *Macromolecules*, 2013, **46**, 9837-9844.

23.   D. R. Tree, Y. Wang and K. D. Dorfman, *Phys. Rev. Lett.*, 2013, **110**, 208103.

24.   A. Muralidhar, D. R. Tree, Y. Wang and K. D. Dorfman, *J. Chem. Phys.*, 2014, **140**,
       084905.

25.   D. Gupta, J. Sheats, A. Muralidhar, J. J. Miller, D. E. Huang, S. Mahshid, K. D.
       Dorfman and W. Reisner, *J. Chem. Phys.*, 2014, **140**, 214901.

26.   L. Dai, J. van der Maarel and P. S. Doyle, *Macromolecules*, 2014, **47**, 2445-2450.

27.   A. Huang and A. Bhattacharya, *Europhys. Lett.*, 2014, **106**, 18004.

28.   M. Chinappi and E. De Angelis, *Philos. Trans. R. Soc. London, A*, 2011, **369**, 2329-
       2336.

29.   C. Micheletti and E. Orlandini, *Macromolecules*, 2012, **45**, 2113−2121.

30.   C. Micheletti and E. Orlandini, *Soft Matter*, 2012, **8**, 10959-10968.

31.   Y.-L. Chen, Y.-H. Lin, J.-F. Chang and P.-k. Lin, *Macromolecules*, 2014, **47**,
       1199−1205.

32.   P. Cifra, *J. Chem. Phys.*, 2012, **136**, 024902.

33.   L. Dai, J. J. Jones, J. R. C. Van der Maarel and P. S. Doyle, *Soft Matter*, 2012, **8**,
       2972-2982.

34.   D. R. Tree, F. R. Wesley and K. D. Dorfman, *Macromolecules*, 2014, **47**, 3672–3368.

35.   F. Brochard and P.-G. De Gennes, *J. Chem. Phys.*, 1977, **67**, 52-56.

36.   H. Nakanishi, *J. Phys. Fr.*, 1987, **48**, 979-984.

37.   P. Cifra, Z. Benková and T. Bleha, *Faraday Discussions*, 2008, **139**, 377-392.

38.   A. Milchev and K. Binder, *Macromolecules*, 1996, **29**, 343-354.

39.   H. Fynewever and A. Yethiraj, *J. Chem. Phys.*, 1998, **108**, 1636-1644.

40.   P. Cifra and T. Bleha, *Polymer*, 2007, **48**, 2444-2452.

41.   I. Ali, D. Marenduzzo and J. M. Yeomans, *Phys. Rev. Lett.*, 2006, **96**, 208102.

42.   H.-P. Hsu, W. Paul and K. Binder, *J. Chem. Phys.*, 2012, **137**, 174902.

43.   Z. Benková and P. Cifra, *Macromolecules*, 2012, **45**, 2597−2608.

44.   I. Teraoka, P. Cifra and Y. Wang, *Colloid. Surface. A*, 2002, **206**, 299-303.

45.   D. I. Dimitrov, A. Milchev, K. Binder, L. I. Klushin and A. M. Skvortsov, *J. Chem. Phys.*, 2008, **128**, 234902.

46.   D. R. Tree, Y. Wang and K. D. Dorfman, *Biomicrofluidics*, 2013, **7**, 054118.

47.   T. A. Witten and P. A. Pincus, *Structured Fluids. Polymers, Colloids, Surfactants*, Oxford University, Oxford, 2004.

48.   I. Teraoka, *Polymer solutions: an introduction to physical properties*, J. Wiley, New York, 2002.

49.   T. Odijk, *Phys. Rev. E*, 2008, **77**, 060901(R).

50.   F. Brochard-Wyart, T. Tanaka, N. Borghi and P.-G. de Gennes, *Langmuir*, 2005, **21**, 4144-4148.

51.   L. Turban, *J. Phys. II Fr.*, 1984, **45**, 347-353.

52.   P. Cifra and T. Bleha, *Soft Matter*, 2012, **8**, 9022-9028.

53.   M. Rubinstein and R. H. Colby, *Polymer Physics*, Oxford University, New York, 1st edn., 2003.

54.   D. R. Tree, A. Muralidhar, P. S. Doyle and K. D. Dorfman, *Macromolecules*, 2013, **46**, 8369−8382.

55.   J. Rémi, *J. Phys. I Fr.*, 1992, **2**, 759-770.

56.   F. Wagner, G. Lattanzi and E. Frey, *Phys. Rev. E*, 2007, **75**, 050902(R).